Interaction of Antimicrobial Peptides, BP100 and pepR, With Model Membrane Systems as Explored by Brownian Dynamics Simulations on a Coarse-Grained Model

Carla S. Alves,[1] Visvaldas Kairys,[1]* Miguel A. R. B. Castanho,[2] Miguel X. Fernandes[1]

[1]*Centro de Química da Madeira, Universidade da Madeira, Campus Universitário da Penteada, 9000-390 Funchal, Portugal*

[2]*Instituto de Medicina Molecular, Faculdade de Medicina, Universidade de Lisboa, 1649-028 Lisbon, Portugal*

Received 26 January 2012; revised 25 March 2012; accepted 10 April 2012
Published online 30 April 2012 in Wiley Online Library (wileyonlinelibrary.com). DOI 10.1002/bip.22075

ABSTRACT:

This work focuses on the conformational and dynamic properties of the antimicrobial peptides (AMPs), BP100 and pepR, when confined within model membrane systems. Brownian dynamics (BD) simulations of a coarse-grained model of each respective peptide in an environment reproducing the phospholipid bilayer were carried out. Simple mean-field potentials were used to reproduce three physically different model phosphatidylcholine (PC) membrane systems. Based on the simplicity of the peptide-membrane models used, 1 μs simulations were performed. With the appropriate choice of parameters, the structure and dynamics of each peptide were recovered from each of the simulated BD trajectories. BP100 was observed to adopt a α-helical conformation when confined in each PC membrane. For pepR under the same conditions, the formation of an N-terminal α-helix was detected, whereas the C-terminus appeared to be less ordered. The dynamic properties of each peptide were characterized in terms of local and global motions. BP100 tended to localize with no preferred orientation approximately halfway across each membrane leaflet, whereas pepR localized near the membrane core with no preferred orientation. Overall, the peptide dynamics were found to vary according to the size of the peptide, as well as the width of the membrane environment. © *2012 Wiley Periodicals, Inc. Biopolymers (Pept Sci) 98: 294–312, 2012.*

Keywords: antimicrobial peptide; Brownian dynamics simulation; coarse-grained model; mean-field potential; membrane model

This article was originally published online as an accepted preprint. The "Published Online" date corresponds to the preprint version. You can request a copy of the preprint by emailing the Biopolymers editorial office at biopolymers@wiley.com

Correspondence to: Miguel X. Fernandes, Centro de Química da Madeira, Universidade da Madeira, Campus Universitário da Penteada, 9000-390 Funchal, Portugal; e-mail: mxf@uma.pt

*Present affiliation: Institute of Biotechnology, Department of Bioinformatics, Vilnius University, Graičiūno 8, Vilnius LT-02241, Lithuania

Contract grant sponsor: Fundação para Ciência e Tecnologia (FCT)
Contract grant number: SFRH/BD/24547/2005
Contract grant sponsor: Portuguese Government
Contract grant number: PEst-OE/QUI/UI0674/2011

INTRODUCTION

An important factor to consider when exploring the potential of antimicrobial peptides (AMPs) as antimicrobial agents is their ability to target and destroy the pathogen while leaving the host intact. The activity of AMPs is known to be directly related to their interaction with the membrane bilayer.[1,2] Mammalian cell and plant cell membranes are mainly composed of zwitterionic phosphatidylcholine (PC) lipids, whereas the outer envelope of bacterial cells contains a significant amount of anionic components (e.g., the phosphate groups of the lipopolysaccharide molecules of Gram-negative bacteria and the lipoteichoic acids found on the surfaces of Gram-positive bacteria).[2,3] As most AMPs are highly cati-

onic, the selective electrostatic binding of these molecules to the negatively charged components of the bacterial membrane is favored.[1,3] The amphipathic nature of the AMP structure subsequently promotes peptide insertion into the hydrophobic core of the bacterial membrane.[1,3] Disruption of the microbial membrane as a result of these direct peptide-lipid interactions then follows, either by an orderly pore-forming mechanism (barrel-stave or toroidal pore models) or by the disordered binding of several peptide molecules to the membrane surface eventually causing membrane destabilization (carpet model).[1,3] Irrespective of the membrane perturbation model adopted, a threshold peptide concentration is always required for membrane disruption to occur.[3,4] Additional or complementary mechanisms accounting for the antimicrobial properties of some AMPs also exist, ranging from cytoplasmic invasion to interference of core metabolic functions.[1] In such mechanisms, the cell membrane must still be traversed for the peptides to reach their target site. Investigating the interaction of the AMPs at the membrane level is thus fundamental in understanding the mode of action of these molecules.

Two distinctly different AMPs form the focus of this work. The first peptide, BP100 (KKLFKKILKYL-NH_2), is a short cationic cecropin A-melittin hybrid peptide[5] designed using a combinatorial chemistry approach.[6] This AMP has been demonstrated to effectively inhibit in vitro the growth of the Gram-negative bacteria *Erwinia amylovora*,[6] *Pseudomonas syringae* pv. *syringae*,[6] *Xanthomonas axonopodis* pv. *vesicatoria*,[6] and *Escherichia coli*,[7] as well as in vivo the growth of *E. amylovora*.[6] BP100 has also been shown to exhibit minimal cytotoxicity[6,8] and low susceptibility to proteinase K degradation.[6] The second peptide, pepR (LKRWGTIKKSKAINVLRGFRKEIGRMLNILNRRRR), is an AMP derived from the RNA binding domain of the dengue virus capsid protein.[9] This considerably more cationic and basic peptide has been shown to effectively inhibit in vitro the growth of *E. coli*.[7]

Through the application of either biophysical or biological studies, some insights into the mode of action of BP100 and pepR have been revealed. A strong selectivity toward anionic bacterial membrane models was reported for BP100, with surface charge neutralization, permeabilization, and translocation being identified as the key processes adopted by this peptide.[8] An important finding of this study was the observation that when using peptide concentrations in the range of that required for microbial inhibition,[6] saturation and consequently surface charge neutralization of the model bacterial membranes occurred.[8] This phenomenon was recently reproduced in the biological setting for both BP100 and pepR.[7] Following the treatment of *E. coli* cells with increasing concentrations of either BP100 or pepR, a strong correlation between the minimal inhibitory concentration (MIC) of each AMP and bacterial surface charge neutralization was revealed. In the same study, the acquisition of atomic force microscopy (AFM) images of the *E. coli* cells treated with either BP100 or pepR under varying conditions allowed for visual insights into these MIC-associated events.[7] Based on the membrane disruption events recorded in the AFM images, the adoption of a carpet-like or detergent-like mechanism by the two AMPs when targeting the Gram-negative *E. coli* bacterial envelope was proposed. Despite the available data on the interaction of either BP100 or pepR with different membrane systems, details on the conformation and dynamic properties adopted by either AMP still need to be elucidated.

Over the past decade, molecular dynamics (MD) simulations have been increasingly used to explore the molecular-level interactions of a range of different peptides with different lipid membranes.[10–18] The use of this strategy has allowed for the acquisition of atomically detailed information on the molecular energetics, structure, and dynamics of these molecules when in the membrane environment. Because of the detailed representation used by MD, however, short timescale trajectories, of only a few hundred picoseconds are possible, that do not reflect the timescales characteristic of physiologically relevant events. An alternative approach to overcome the time limitations imposed by all-atomic simulation methods is the implementation of simple, low-molecular detail models; the dynamics of which can be described by the laws of Brownian motion.[19] Although not as predictive as all-atom representations, the use of coarse-grained models have been demonstrated to effectively simulate the behavior of proteins and other biomolecular molecules on mesoscopic size scales and timescales.[20] Chang et al.,[21] for example, were able to apply 1 μs Brownian dynamics (BD) simulations on a coarse-grained model to study the gated association rate constants for wild-type and mutant human immunodeficiency virus type 1 proteases. The applied methodology was found to be efficient, and the computed association rate constants yielded through this approach were in good agreement with the experimentally derived values. The same methodology has since been successfully applied to investigate the channeling of an intermediate APS^{2-} substrate in a sulfate-activating complex for a

Correspondence to: Miguel X. Fernandes, Centro de Química da Madeira, Universidade da Madeira, Campus Universitário da Penteada, 9000-390 Funchal, Portugal; e-mail: mxf@uma.pt
*Present affiliation: Institute of Biotechnology, Department of Bioinformatics, Vilnius University, Graičiūno 8, Vilnius LT-02241, Lithuania
Contract grant sponsor:
*Present affiliation: Institute of Biotechnology, Department of Bioinformatics, Vil-

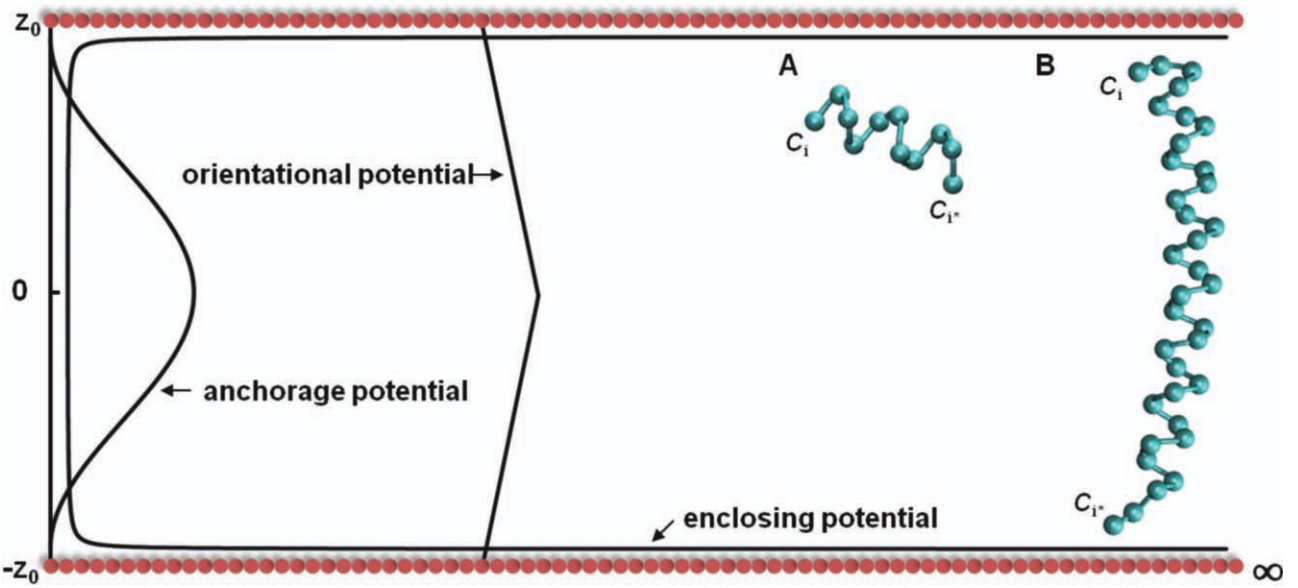

FIGURE 1 Schematic representation of the coarse-grained model of (A) BP100 and (B) pepR in the membrane environment. The profiles of the mean-field potentials used to describe the behavior of the peptide models when confined within the membrane environment are shown.

total trajectory time of 3–5 μs.[22] Through the application of a simple mean-field approach and BD simulations, Fernandes et al. were also able to accurately describe the dynamics of a 1,2-dipalmitoyl-*sn*-glycero-3-phosphocholine (DPPC) bilayer system in the liquid-crystal phase (L_α)[23] and in the gel phase (L_β)[24] in the microsecond timescale. The conformational and dynamic properties of a single hydrocarbon chain[23,24] and a *trans*-parinaric acid molecule[24] embedded in the different DPPC environments were also correctly predicted using this mean-field approach.

In this study, the coarse-grained model reported by Chang et al.[21] and the mean-field approach developed by Fernandes et al.[23,24] were applied in combination to explore the conformational and dynamic properties of both BP100 and pepR in different membrane systems. The interactions of each AMP with model membrane systems mimicking either mammalian cell or bacterial cell membranes were considered. The models selected to mimic the mammalian cell membrane were 1-palmitoyl-2-oleyl-*sn*-glycero-3-phosphocholine (POPC) in the liquid-disordered phase and cholesterol-containing POPC (POPC:Chol) in the liquid-ordered phase (L_o), whereas the model mimicking the bacterial cell membrane was 1-palmitoyl-2-oleoyl-*sn*-glycero-3-(phosphor-rac-(1-glycerol)):1-palmitoyl-2-oleyl-*sn*-glycero-3-phosphocholine (POPG:POPC) in the liquid-disordered phase. BD simulations of a coarse-grained model of each AMP when located in any one of these three modeled membrane environments were performed for a time equivalent to 1 μs. A detailed analysis of the conformation adopted by each peptide, as well as the characterization of its local and global motions, when confined in the membrane was performed. Where applicable, the results were compared with the available experimental data. Insights into the structural and dynamic properties of both BP100 and pepR when interacting with the membrane environment were drawn from the BD simulation studies thereby shedding some light into their mode of action.

MATERIALS AND METHODS

Peptide-Membrane Model

The system considered in this study is illustrated in Figure 1. Both BP100 and pepR are represented using a coarse-grained model. For each AMP, each amino acid within its structure is represented as a single spherical interaction center (bead) with an effective radius, σ_i.[21,25–27] The center of each bead is placed onto the C_α atom of each residue within the peptide. Connecting the centers of the consecutive beads of each peptide are virtual bonds, bond angles, and dihedral angles.

The coarse-grained model of the peptide of interest is then placed into a membrane model of finite thickness and is allowed to move. This movement is restricted in the direction of the *z*-axis, which means that the motions of each peptide are confined within the membrane boundaries. To simulate the movement of each peptide confined in the modeled membrane environment, three mean-field potentials are used: (1) the enclosing potential that takes into account the finite thickness of the bilayer, as well as the hydrophilic nature of the membrane interfaces[19,23,24]; (2) the anchorage potential that positions each peptide residue that tends to interact favorably with the membrane interface in its vicinity[23,24]; and (3) the orientational

potential that promotes the correct orientation of the simulated peptide relative to the normal of the membrane interface.[19,23,24]

Peptide Energetics

The coarse-grained force field used to model BP100 and pepR is based on a method developed by Tozzini and McCammon.[26] In the modified method that is used in this study, the force field is extended to include the solvent effects via screened electrostatics.[21]

The potential energy function used to account for the total intramolecular interactions of each peptide is a sum of five interactions and is given by the following equation:

$$U = U_{\text{bond}} + U_{\text{angle}} + U_{\text{dihe}} + U_{\text{vdw}} + U_{\text{elec}}. \quad (1)$$

The bond interaction energy, U_{bond}, is defined by a harmonic potential that maintains the equilibrium bond length between any two consecutive C_α atoms. It is expressed as follows:

$$U_{\text{bond}} = \sum_{\text{bonds}} k_b (b - b_0)^2, \quad (2)$$

where k_b is the spring constant, b is the instantaneous distance between two consecutive beads, and b_0 is the equilibrium bond distance.

The bond angle interaction energy, U_{angle}, which maintains the equilibrium bond angle between any three consecutive C_α atoms, is given by the following quartic expression:

$$U_{\text{angle}} = \sum_{\text{angles}} \tfrac{1}{2} k_\theta (\theta - \theta_0)^2 + \tfrac{1}{3} k'_\theta (\theta - \theta_0)^3 + \tfrac{1}{4} k''_\theta (\theta - \theta_0)^4, \quad (3)$$

where k_θ, k'_θ, and k''_θ are the bond angle constants, θ is the instantaneous bond angle between three consecutive beads, and θ_0 is the equilibrium bond angle.

The dihedral angle interaction energy, U_{dihe}, also defined by a harmonic potential, has the following expression:

$$U_{\text{dihed}} = \sum_{\text{dihedrals}} k_\phi (\phi - \phi_0)^2, \quad (4)$$

where k_ϕ is the dihedral angle constant, ϕ is the instantaneous dihedral angle between the C_α atoms of four consecutive beads, and ϕ_0 is the equilibrium dihedral angle.

For any pair of nonbonded beads, i and j (pair not involved in any of the previous three interactions), within 15 Å of each other, the van der Waals, U_{vdw}, and Coulombic, U_{elec}, interaction energy contributions are considered. The expression for each contribution is as follows:

$$U_{\text{vdw}} = \sum_{\substack{\text{nonbonded} \\ \text{atom pairs}}} \in \left[\left(1 - e^{-\alpha (r_{ij} - r_0)} \right)^2 - 1 \right] \quad \text{for } r_{ij} \leq 15\text{Å}, \quad (5)$$

$$U_{\text{elec}} = \sum_{\substack{\text{nonbonded} \\ \text{atom pairs}}} \left(\frac{q_i q_j}{\varepsilon_D r_{ij}} \right) \quad \text{for } r_{ij} \leq 15\text{Å}, \quad (6)$$

where for both contributions, r_{ij} represents the distance between the C_α atoms of beads i and j. For the van der Waals interaction, $\in$ and α are parameters defined by the force field, and r_0 is the equilibrium distance between the nonbonded pair of beads. When considering the Coulombic interaction, a charge q of $\pm 1e$ is assigned to each charged residue. This potential energy contribution was later extended by Chang et al.[21] to include solvent effects via screened electrostatics. This was achieved using a distance-dependent dielectric constant ($\varepsilon_D = 4r_{ij}$) to avoid unrealistic in vacuo Coulombic interactions when performing the BD simulations.

Membrane Energetics

To describe the membrane environment in which the coarse-grained model of the peptide of interest moves, three mean-field potentials are considered, namely, the enclosing potential,[19,23,24] the anchorage potential,[23,24] and the orientational potential.[19,23,24] The expression for each contribution is as follows:

$$U_{\text{encl}} = \sum \frac{k_B T K_z}{(z_0^2 - z_i^2)}, \quad (7)$$

$$U_{\text{anch}} = \sum k_B T K_\theta \cos^2 \left(\frac{z_i \pi}{2 z_0} \right), \quad (8)$$

$$U_{\text{orient}} = \sum -\frac{3}{2} k_B T K_\theta \left(\cos^2 \theta_i - 1 \right), \quad (9)$$

where k_B is the Boltzmann constant and T is the temperature. For both U_{encl} [Eq. (7)] and U_{anch} [Eq. (8)], z_0 is the half-width of the membrane and z_i is the z-coordinate of the C_α atom of bead i in the peptide. For U_{orient} [Eq. (9)], θ_i is the tilt angle that is formed between the z-axis and the vector that joins the two beads at the extremities of the peptide fragment to be orientated (beads C_i and C_{i^*} in Figure 1). The parameters K_z, K_θ, and K_θ represent the field strengths of the enclosing, anchorage, and orientational potentials, respectively. Depending on the physical characteristics of the membrane model under investigation, the magnitude of each potential varies. When compared with bilayers in the L_β phase, K_z is higher, K_θ is lower, and K_θ is lower for bilayers in the L_α phase.[24]

To maintain either BP100 or pepR enclosed within the membrane boundary, U_{encl} [Eq. (7)] was applied onto each residue of the simulated peptide. The mean-field potentials U_{anch} [Eq. (8)] and U_{orient} [Eq. (9)] were also applied onto each residue of the simulated peptides.

BD Simulation Method

For each AMP investigated in this study, the Brownian trajectory of a single peptide molecule in a model membrane system was determined. The algorithm reported by Iniesta and García de la Torre,[28] which is based on the method developed by Ermak and McCammon,[29] was used here to solve the trajectory of each peptide. In the method used, each BD step was taken into account twice in a predictor-corrector manner (for more details see Ref. 28).

When simulating the BD trajectories for each respective AMP, the so-called hydrodynamic interaction (HI) between residues in a molecule was determined. As the dynamic behavior of each AMP

Table I Physical Properties of the Modeled Membrane Systems Used in the BD Simulation Studies

	Membrane Model	Membrane Half-Width, z_0 (Å)	Viscosity, η (cP)	Temperature, T (K)	Tilt Angle, θ_i (°)
L_α	POPC	20.0[33]	1.5[34]	293[35]	46.5[35]
L_o	POPC:Chol	20.0[33]	2.0[34]	293[35]	44.5[35]
L_α	POPG:POPC	21.5[36]	1.5	293	46.5

confined within the membrane environment was only explored in this study, the HI between residues was dependent on the viscosity of the membrane environment only (i.e., η_m). Thus, the diffusion tensor, $\boldsymbol{D}_{ii}$, of the system was considered to take on the value of k_BT/ξ_m. For the determination of the HI between two residues, $\boldsymbol{D}_{ij}$ ($i \neq j$) was calculated using the Rotne-Prager-Yamakawa (modified Oseen) tensor[30,31] that corrects for the effects of the nonpoint-like nature of frictional elements, as well as eventual overlapping.

Parameterization of Simulated System

The coarse-grained force field parameters used to model each AMP were determined using a systematic search. For each peptide model, the following force field parameters were selected: $k_b = 70$ kcal/(mol Å^2),[21] $b_0 = 3.81$ Å,[21] $k_\theta = 38$ kcal/(mol rad^2),[21] $k'_\theta = -3.4$ kcal/(mol rad^2), $k_\phi = 7.5$ kcal/(mol rad^2), $\epsilon = 0.33$ kcal/mol,[32] $\alpha = 0.70711$ Å^{-1},[21] and $r_0 = 6.3$ Å.[32] The optimal θ_0 and ϕ_0 values for either BP100 or pepR were dependent on each bonded amino acid unit within the peptide structure.

The physical properties of each of the simulated membrane models are listed in Table I. The membrane half-width (z_0) and viscosity (η) values were selected according to the physical properties of each system at a given temperature. For POPG:POPC in the L_α phase, these values were selected based on the properties of the membrane at 293 K. To describe the orientation of each AMP relative to the membrane normal, the tilt angle (θ_i) values reported for the cell-penetrating peptide (CPP), Pep-1, in POPC and POPC:Chol were used here.[35] Based on the similar physical properties of POPG:POPC (L_α) relative to POPC (L_α),[37] an equivalent θ_i value was selected for each peptide when simulated in the POPG:POPC membrane model. The mean-field potential constants parameterized by Fernandes et al.[23] for DPPC in the L_α phase were adopted to simulate POPC (L_α), POPC:Chol (L_o), and POPG:POPC (L_α). Here, the enclosing potential constant, K_z, was set at 4.63 kcal Å^2/mol, the anchorage potential constant, K_θ, used was 2.32×10^{-2} kcal/mol, and the orientational potential constant, K_θ, used was 1.24×10^{-2} kcal/mol.

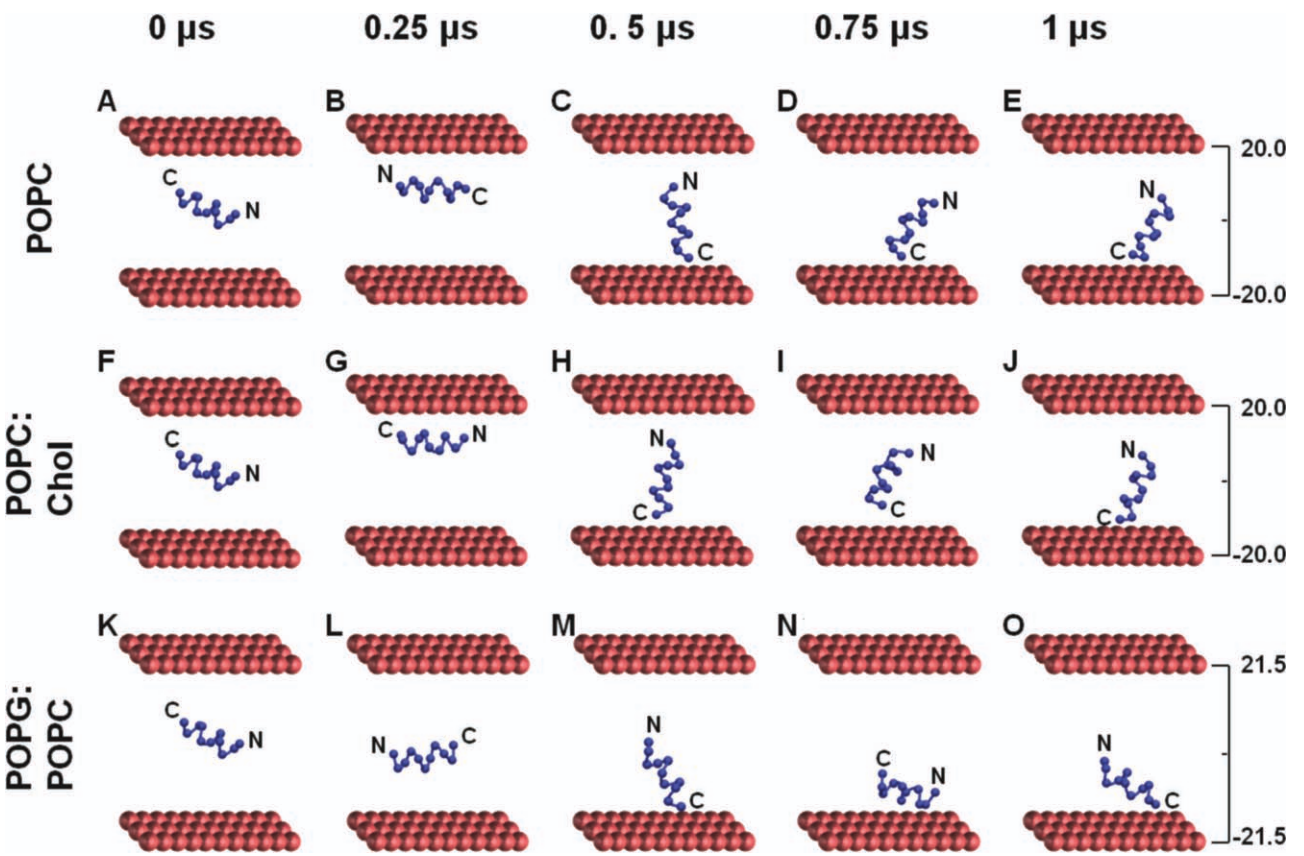

FIGURE 2 BD simulation of BP100 in POPC (L_α) (A–E), POPC:Chol (L_o) (F–J), and POPG:-POPC (L_α) (K–O). Frames taken at 0, 0.25, 0.50, 0.75, and 1 μs are shown. In all instances, the N- and C-termini of the peptide are highlighted.

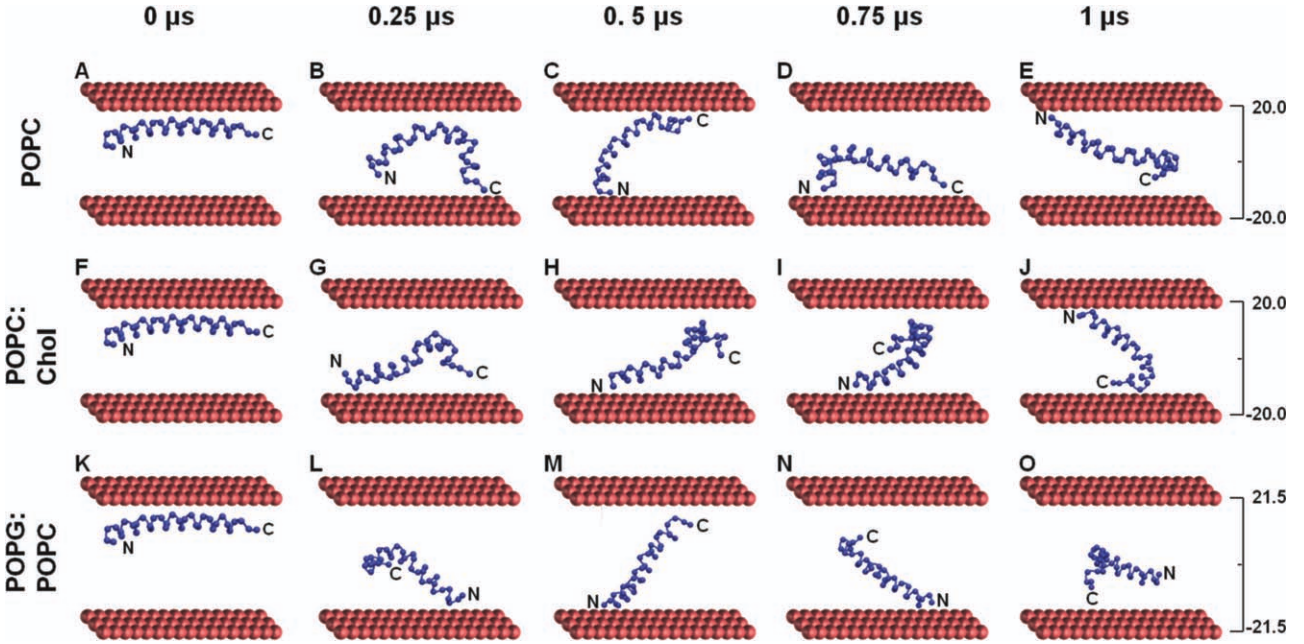

FIGURE 3 BD simulation of pepR in POPC (L_α) (A–E), POPC:Chol (L_o) (F–J), and POPG:-POPC (L_α) (K–O). Frames taken at 0, 0.25, 0.50, 0.75, and 1 μs are shown. In all instances, the N- and C-termini of the peptide are highlighted.

Simulation and Evaluation

The BD trajectories generated for both BP100 and pepR were simulated using a computation time step (dt) of 1.0 fs, for a total trajectory time of 1 μs. The trajectories were sampled at 100 ps intervals, and structural features such as the backbone dihedral angles, end-to-end distances, and helix length were analyzed. For each structural property investigated, an average over the entire trajectory was measured.

For the determination of the dynamic properties of each AMP, the BD trajectories were also sampled at 100 ps intervals. The local and global peptide motions were monitored along each of the simulated BD trajectories, and the translational dynamics of each peptide under the varying conditions was determined. To determine the translational dynamics of each respective AMP, the lateral diffusion coefficient was extracted from the mean-square displacement of the peptide mass center using the following equation:

$$\lim_{t\to\infty} \langle \alpha^2(t) \rangle = 4Dt, \tag{10}$$

where the average for the x- and y-coordinates is measured over any possible choice of the initial time, that is,

$$\alpha^2(t) = [x(t) - x(0)]^2 + [y(t) - y(0)]^2. \tag{11}$$

RESULTS

Structural Properties of BP100 and pepR

To gain insights into the structural properties of both BP100 and pepR when confined within the membrane environment, BD simulations of each peptide in POPC (L_α), POPC:Chol (L_o), or POPG:POPC (L_α) were performed. The 1 μs BD trajectories were sampled at regular intervals, and the peptide structures were assessed at each point. Figures 2 and 3 show the snapshots taken at 0, 0.25, 0.5, 0.75, and 1 μs for BP100 and pepR, respectively, under the various conditions. Analysis of the structure of BP100 in the different membrane environments pointed to the adoption of a α-helix (see Figure 2). For pepR under the same conditions, variations in its conformation were evident. Overall, the formation of a α-helix at the N-terminus of this peptide was clear, whereas the C-terminus appeared to be less ordered (see Figure 3).

To confirm the detection of a α-helical component, the C_α dihedral angles of each AMP were closely assessed. These dihedral angles are defined by four consecutive C_α atoms, starting at the ith bead in the peptide model. The average C_α dihedral angles and the corresponding root-mean-square-deviation (RMSD) values for each amino acid of BP100 and pepR when simulated in POPC are shown in Figures 4A and 4B, respectively. The C_α dihedral angles recorded for each amino acid of BP100 were observed to fluctuate between 50.8° and 58.2°, with each dihedral angle exhibiting a negligible RMSD (Figure 4A). For pepR, on the other hand, only the C_α dihedral angles for residues 2–27 were observed to fluctuate around 48.6° ± 5.2° (Figure 4B). In this region, RMSD values of ~2.6° were detected. The remaining pepR C_α dihedral angles, at both ends of the peptide, deviated from 50° to varying degrees and exhib-

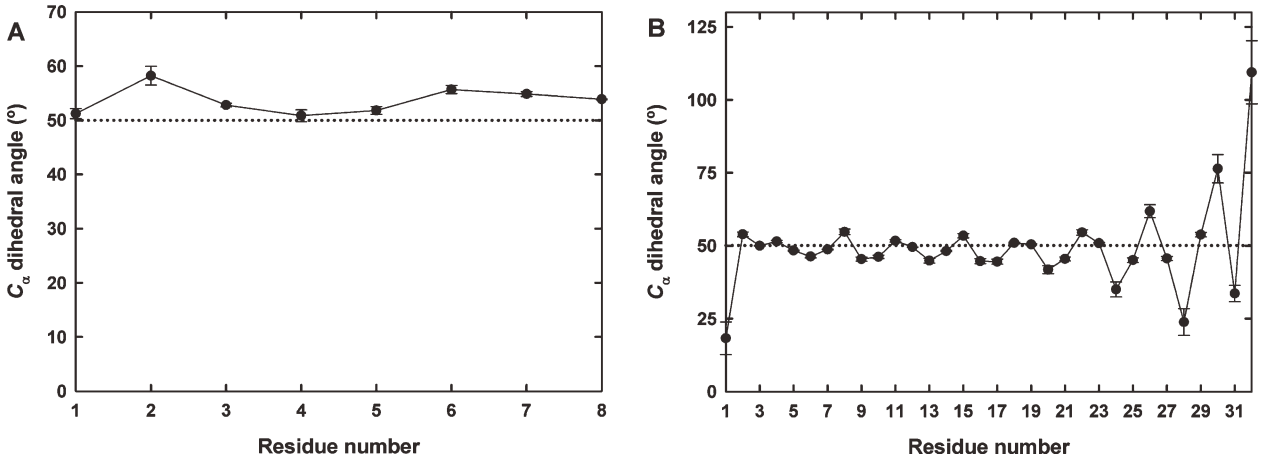

FIGURE 4 The average C_α dihedral angles for (A) BP100 and (B) pepR when simulated in POPC. The dihedral angles are defined by the first (i) and the fourth ($i + 3$) C_α atoms of four consecutive C_α atoms, starting at the ith bead in the peptide model. The dotted lines indicate the typical C_α dihedral angle value for an ideal α-helix. Error bars indicate the RMSD values.

ited RMSD values at least eight times larger than those in the region encompassing residues 2–27 (Figure 4B). The simulation of either BP100 or pepR when confined in any one of the two remaining membrane models revealed equivalent trends to that demonstrated in the respective graphs in Figure 4.

Further analysis of the BD trajectories revealed key structural features for both BP100 and pepR when confined in the membrane environment. The snapshots presented in Figures 5A and 5B are typical for BP100 and pepR, respectively, when simulated in any one of the three different modeled membrane systems. For BP100, the charged and hydrophobic residues were observed to segregate along the helix diameter (Figure 5A). Analysis of the simulated pepR structure (Figure 5B), on the other hand, demonstrated amphipathic segments along the peptide structure.

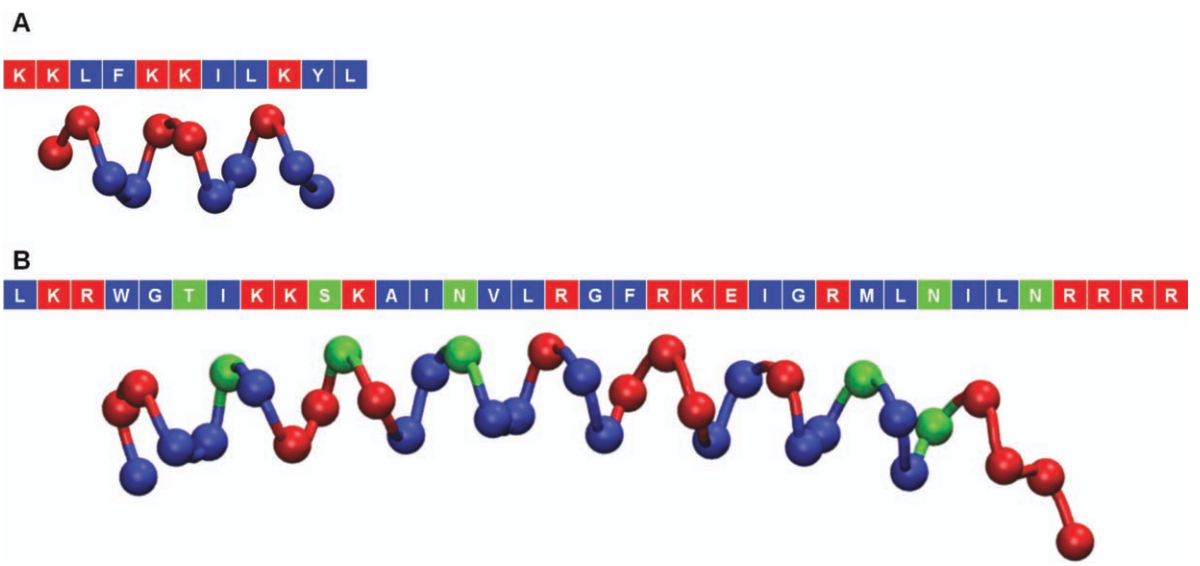

FIGURE 5 Simulation snapshots depicting the structures typical for (A) BP100 and (B) pepR when simulated in the modeled membrane environments. It should be noticed that for BP100, the charged and hydrophobic residues are observed to be distributed onto opposite regions of the structure. For pepR, on the other hand, the distribution of the charged and hydrophobic residues onto opposite regions of the structure is only detectable in some portions within the peptide. Hydrophobic residues are represented in blue, noncharged polar in green, and charged polar in red.

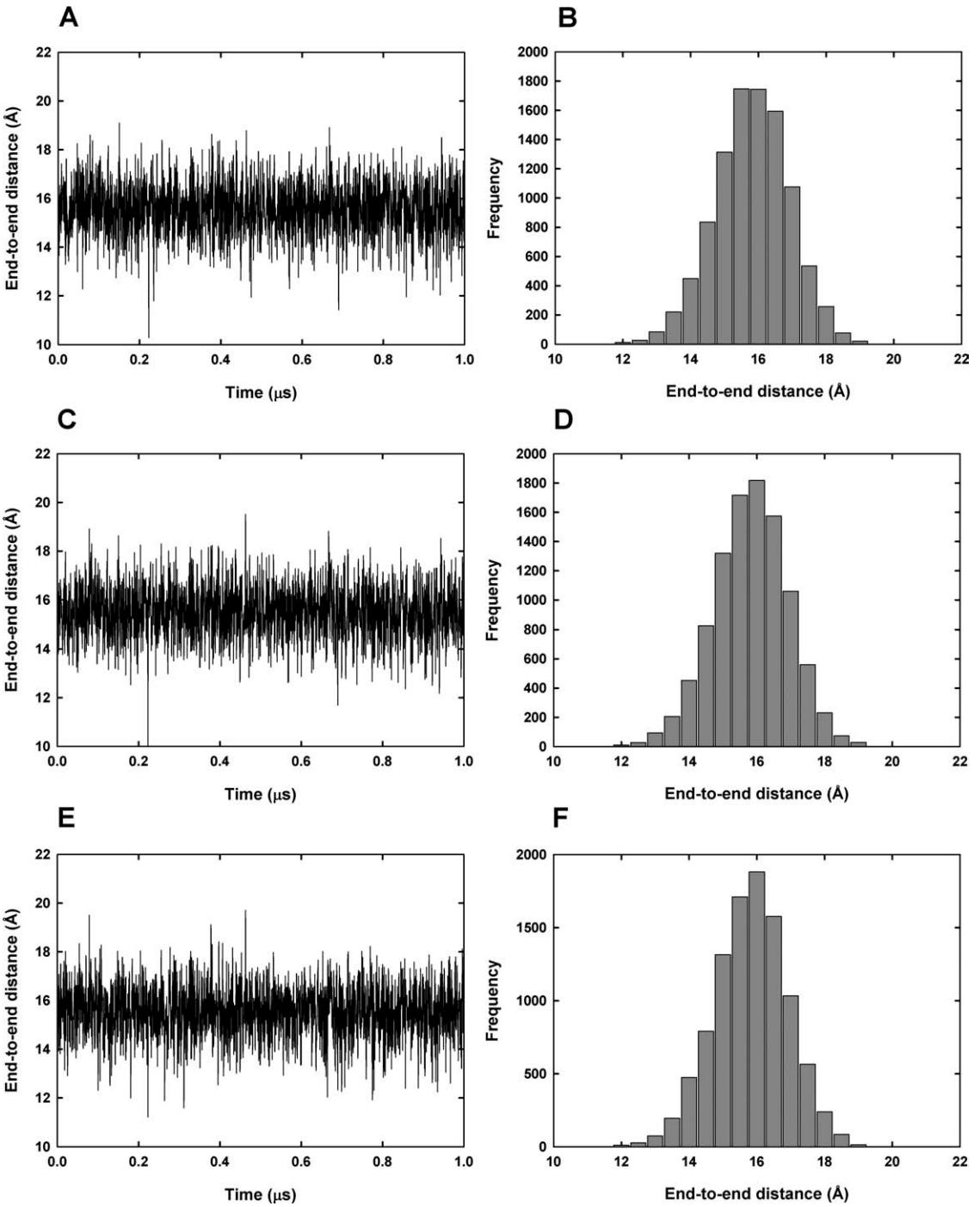

FIGURE 6 The time evolution profiles and corresponding probability distribution curves of the end-to-end distance between the N- and C-terminal residues of BP100 when simulated for 1 μs in POPC (L_α) (A and B), POPC:Chol (L_o) (C and D), and POPG:POPC (L_α) (E and F).

Dynamic Properties of BP100 and pepR

Local Peptide Motions. To verify the above-described observations and to gain further insights into the overall structural properties of both BP100 and pepR, key structural elements were screened for each peptide throughout each of the simulated BD trajectories.

For BP100, the distance between the N- and C-terminal residues of the peptide when simulated in POPC (L_α), POPC:Chol (L_o), or POPG:POPC (L_α) was measured. Figure

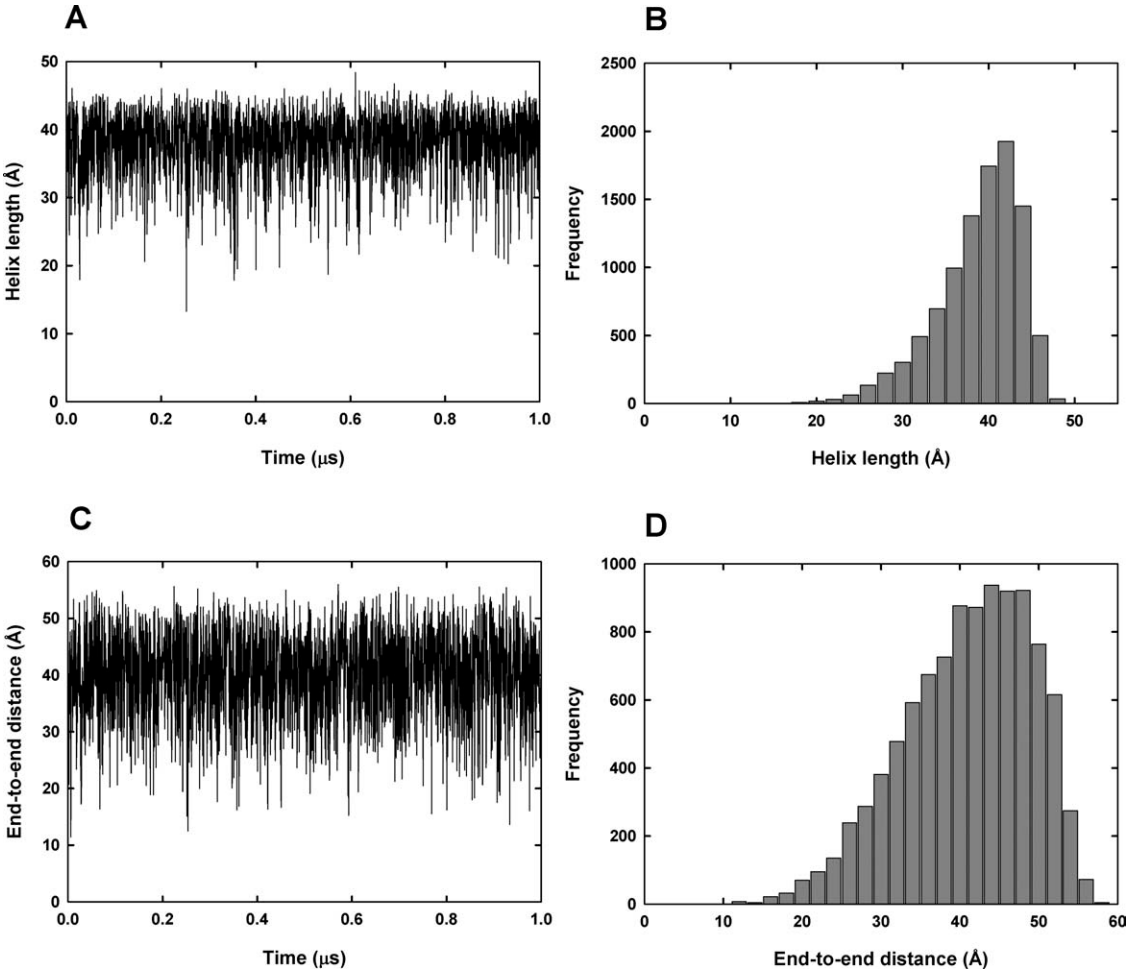

FIGURE 7 Local motions of pepR when simulated for 1 μs in POPC (L_α). The time evolution profiles and corresponding probability distribution curves of the length of the peptide N-terminal α-helix (A and B) and the end-to-end distance between the N- and C-termini of the peptide (C and D).

6 shows the time evolution of the end-to-end distance between the two terminal residues of the peptide when simulated in the three modeled membrane environments. The corresponding probability distribution curves are also illustrated. In all instances, the distance measured between Lys1 and Leu11 were comparable, fluctuating between 9.8 and 20.3 Å (Figures 6A, 6C, and 6E). The average measured distance between these two residues was 15.57 ± 1.10 Å, 15.57 ± 1.10 Å, and 15.58 ± 1.08 Å for BP100 in POPC (L_α) (Figure 6B), POPC:Chol (L_o) (Figure 6D), and POPG:POPC (L_α) (Figure 6F), respectively.

For pepR, on the other hand, two structural components were screened for the peptide throughout each of the simulated BD trajectories: (1) the length of the N-terminal α-helix and (2) the end-to-end distance between the N- and C-termini. Figure 7 shows the time evolution of these two structural properties, accompanied by the corresponding probability distribution curves, for pepR when simulated in POPC (L_α). From Figure 7A, it is clear that the distance between the first (Lys2) and last (Leu30) residues constituting the N-terminal α-helix fluctuated in the range of 13.3–48.4 Å. On average, the helix length measured here was found to be 37.8 ± 4.9 Å (Figure 7B). Equivalent distributions were recorded for pepR when simulated in POPC:Chol (L_o) and POPG:POPC (L_α), with the average measured helix length recorded under these conditions being 37.6 ± 5.1 Å and 37.9 ± 4.9 Å, respectively (graphs not shown).

Analysis of the distance separating the N- and C-termini of pepR when simulated in the membrane environment revealed a similar trend to that described for the N-terminal α-helix. When simulating the peptide in POPC (L_α), for example, the distance between Leu1 and Arg35 was found to be in the range of 9.5–57.6 Å (Figure 7C). The average measured distance in this case was 39.9 ± 8.1 Å (Figure 7D). Sim-

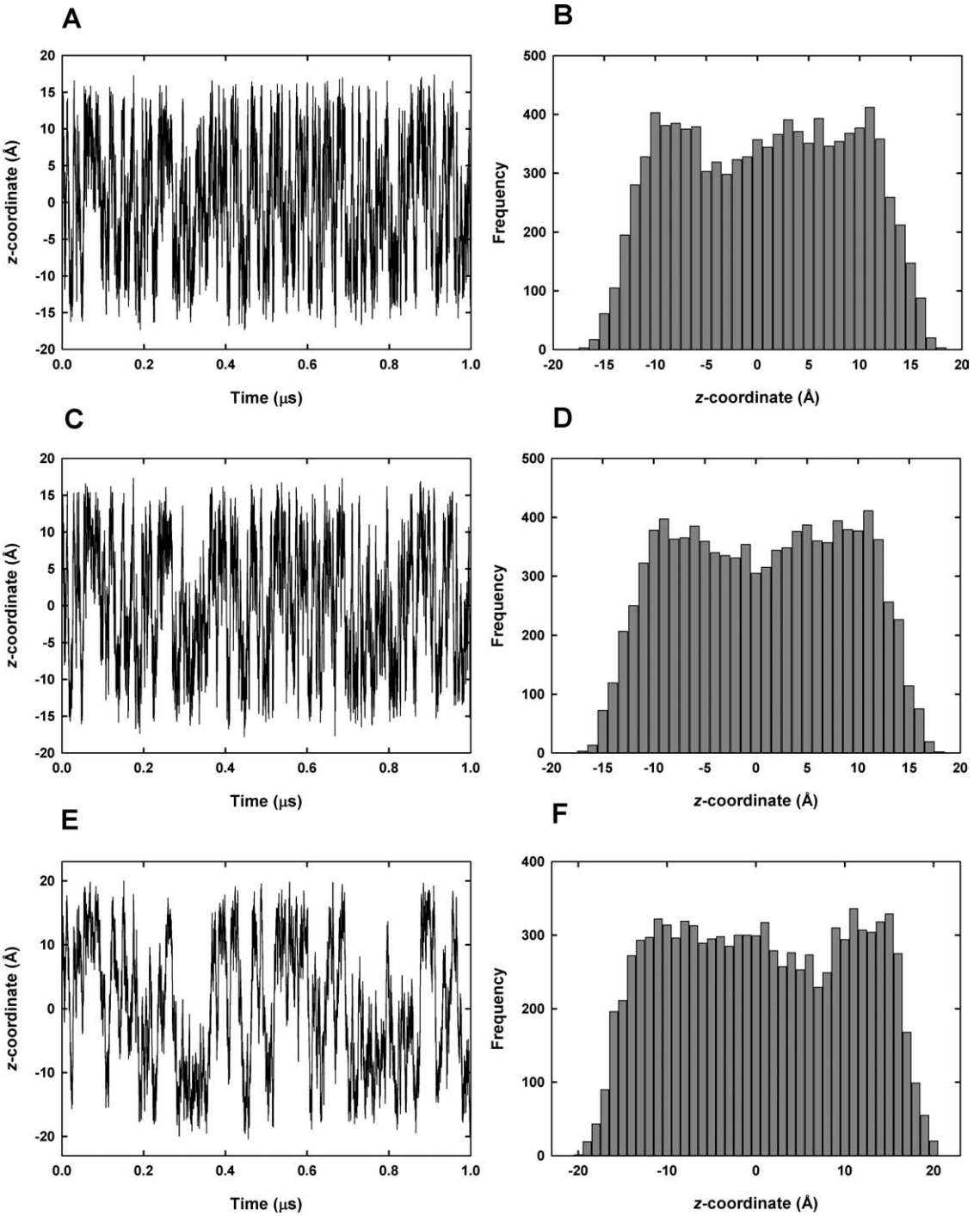

FIGURE 8 The time evolution profiles and corresponding probability distribution curves of the transverse position of the center of mass of BP100 when simulated for 1 μs in POPC (L_α) (A and B), POPC:Chol (L_o) (C and D), and POPG:POPC (L_α) (E and F).

ilar distributions were observed for pepR when simulated in POPC:Chol (L_o) and POPG:POPC (L_α), with the average measured distance between the two terminal residues obtained being 39.6 $\pm$ 8.4 Å and 40.1 $\pm$ 8.1 Å, respectively (graphs not shown).

Global Peptide Motions. To investigate the global motions of both BP100 and pepR when confined within the membrane environment, the localization and orientation of each AMP within the different modeled membrane systems was monitored.

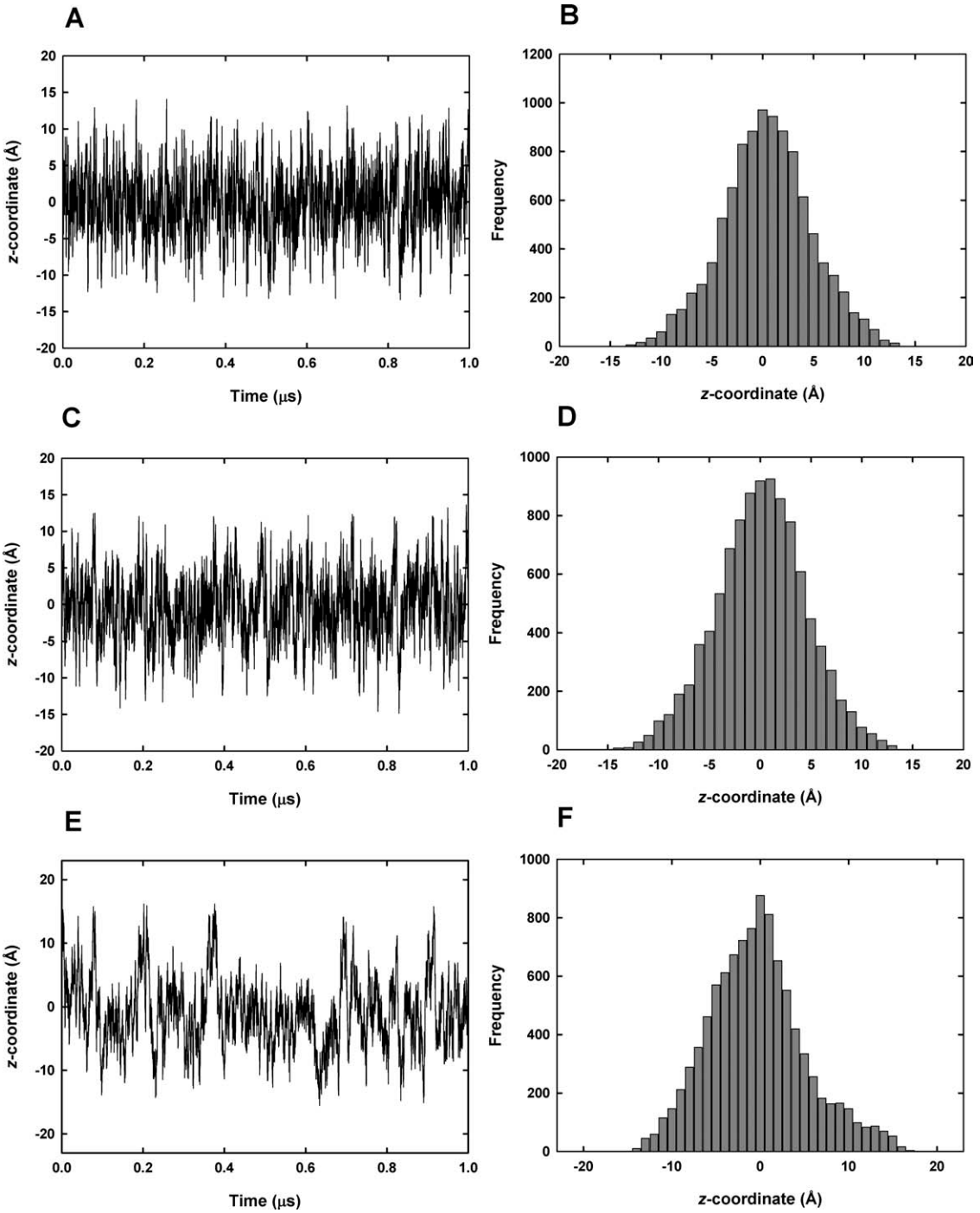

FIGURE 9 The time evolution profiles and corresponding probability distribution curves of the transverse position of the center of mass of pepR when simulated for 1 μs in POPC (L_α) (A and B), POPC:Chol (L_o) (C and D), and POPG:POPC (L_α) (E and F).

Figures 8 and 9 show the time evolution profiles of the transverse position of the center of mass for BP100 and pepR, respectively, when simulated in POPC (L_α), POPC:Chol (L_o), or POPG:POPC (L_α). In each case, the corresponding probability distribution curves are illustrated. Comparison of the time evolution profiles revealed a more frequent fluctuation in the Brownian motion of each AMP when traversing POPC (L_α) (Figures 8A and 9A) and POPC:Chol (L_o) (Figures 8C and 9C) relative to when crossing POPG:POPC (L_α) (Figures 8E and 9E). For

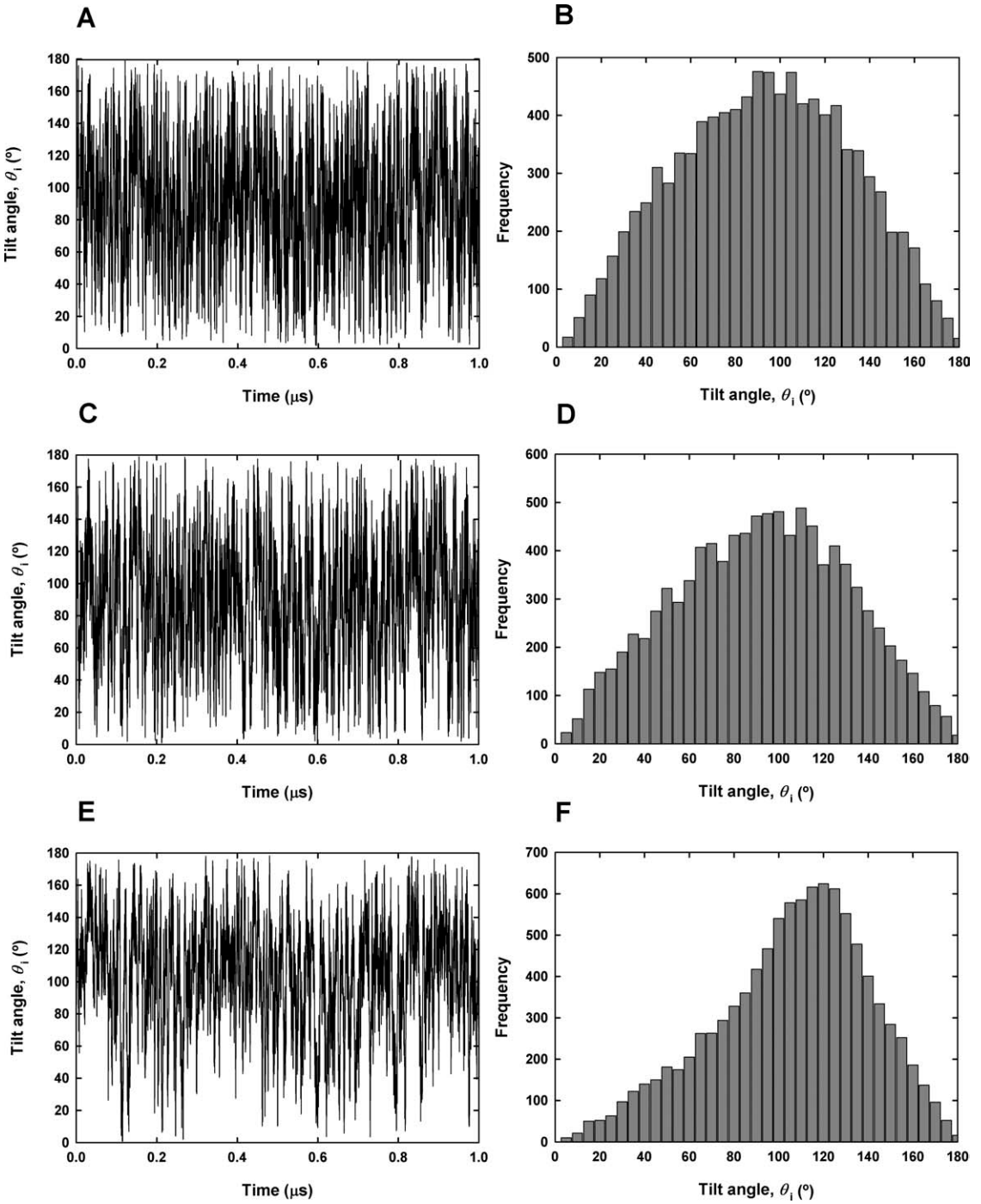

FIGURE 10 The time evolution profiles and corresponding probability distribution curves of the tilt angle, θ_i, adopted by BP100 when simulated for 1 μs in POPC (L_α) (A and B), POPC:Chol (L_o) (C and D), and POPG:POPC (L_α) (E and F).

BP100, this movement was distributed across the *z*-axis of each of the modeled membranes. This is reflected in Figures 8B, 8D, and 8F, by the broad density profiles of the position of the center of mass of the peptide. The manifestation of two peaks at ± 10 Å from the bilayer center in each density profile, however, demonstrates the preferred localization of the peptide approximately halfway across the membrane leaflet. In contrast, the pepR mass center tended to localize preferentially near the bilayer center of each membrane model. The narrow distribution

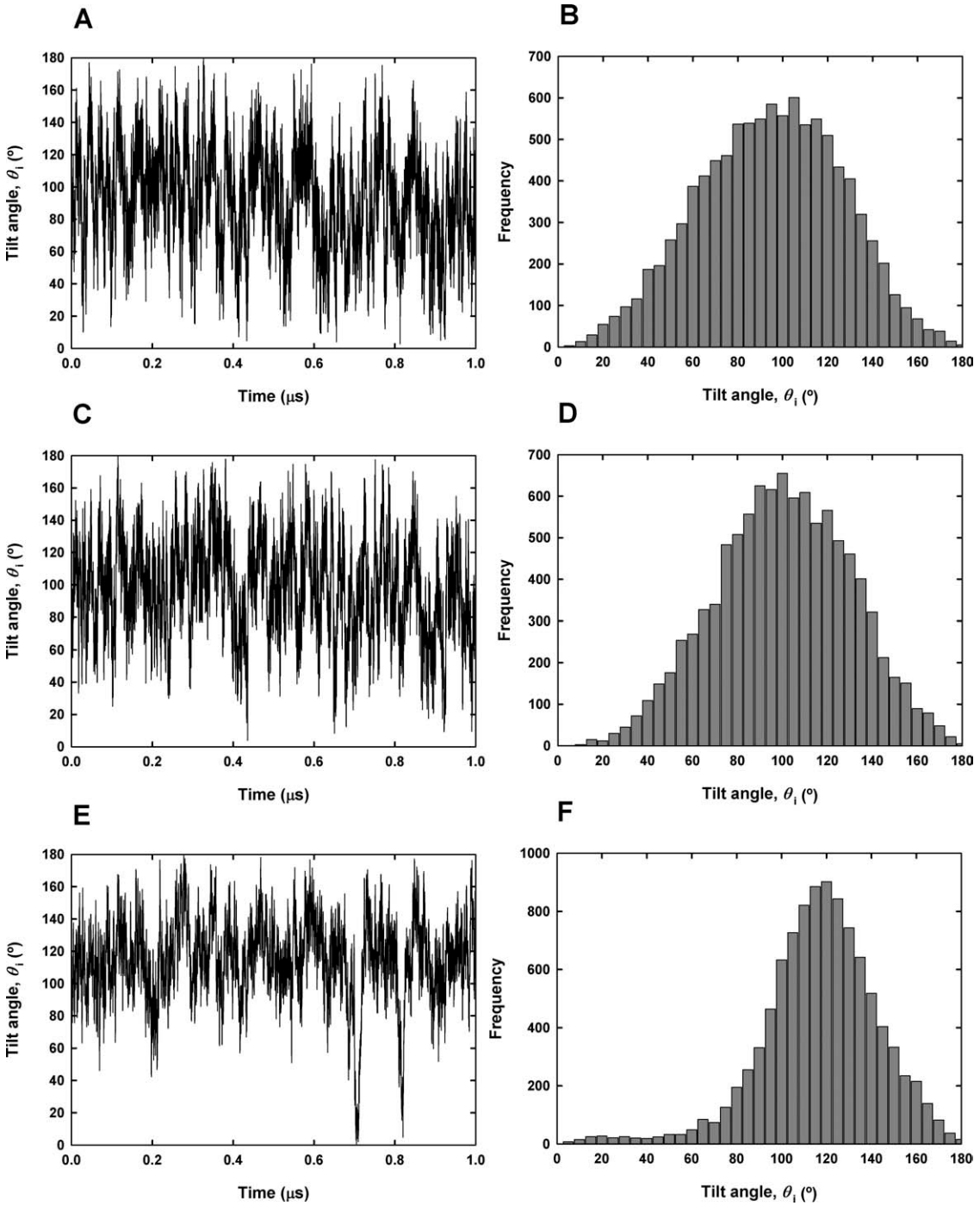

FIGURE 11 The evolution profiles and corresponding probability distribution curves of the tilt angle, θ_i, adopted by pepR when simulated for 1 μs in POPC (L_α) (A and B), POPC:Chol (L_o) (C and D), and POPG:POPC (L_α) (E and F).

of the position of its center of mass around the membrane core, evident in the density profiles in Figures 9B, 9D, and 9F, is indicative of this.

The orientation of each AMP in relation to the membrane normal was similarly monitored and compared. Figures 10 and 11 show the evolution profiles of the tilt angle, θ_i, adopted by BP100 and pepR, respectively, when simulated in POPC (L_α), POPC:Chol (L_o), or POPG:POPC (L_α). The corresponding probability distribution curves for θ_i are also shown. Examination of the evolution of θ_i along

Table II Diffusion Coefficients Recovered for BP100 and pepR When Confined Within the Three Modeled Membrane Environments

	Membrane Model	Diffusion Coefficient, D ($\times 10^{-7}$ cm^2/s)	
		BP100	pepR
L_α	POPC	30.7 ± 14.6	15.0 ± 3.5
L_o	POPC:Chol	17.1 ± 5.7	13.0 ± 4.1
L_α	POPG:POPC	10.8 ± 7.1	7.7 ± 3.5

each of the simulated BD trajectories demonstrated a frequent fluctuation in the orientation of each peptide when in POPC (L_α) (Figures 10A and 11A), POPC:Chol (L_o) (Figures 10C and 11C), and POPG:POPC (L_α) (Figures 10E and 11E). From the distribution profiles, however, it is clear that these fluctuations occurred over a wider domain of orientations in POPC (L_α) (Figures 10B and 11B) and POPC:Chol (L_o) (Figures 10D and 11D) relative to when in POPG:POPC in the L_α phase (Figures 10F and 11F). The average measured tilt angle adopted by BP100 relative to the membrane normal of POPC (L_α), POPC:Chol (L_o), or POPG:POPC (L_α) was 90.5° ± 38.4°, 90.0° ± 38.2°, and 103.0° ± 34.5°, respectively. For pepR, the average tilt angle adopted by the structure relative to the membrane normal of POPC (L_α), POPC:Chol (L_o), or POPG:POPC (L_α) was 91.9° ± 31.7°, 97.8° ± 30.0°, and 114.4° ± 25.8°, respectively.

Peptide Translational Diffusion. The translational diffusion of both BP100 and pepR when confined in POPC (L_α), POPC:Chol (L_o), or POPG:POPC (L_α) was investigated. The diffusion coefficients obtained for each AMP under the various simulation conditions are summarized in Table II. When confined within the different membrane environments, each AMP was observed to display a decrease in its lateral diffusion in the order of POPC (L_α) > POPC:Chol (L_o) > POPG:POPC (L_α). For BP100, an almost threefold decrease in its diffusion in the presence of POPG:POPC (L_α) relative to POPC (L_α) was observed. On the other hand, an almost twofold decrease was observed for pepR when comparing its diffusion coefficient in POPG:POPC (L_α) relative to when in POPC (L_α).

On closer examination, a clear difference in the magnitude of the diffusion coefficients obtained for BP100 and pepR under the equivalent simulation conditions was also evident. Simulation of BP100 in the more fluid membrane model, POPC (L_α), presented a diffusion coefficient approximately two times larger than that of pepR in the same membrane. For BP100 in the slightly thicker POPG:POPC (L_α), however, a diffusion coefficient of 1.4-fold greater than that of pepR in the same membrane model was obtained.

DISCUSSION

To date, the data available on the structural conformation adopted by each of the AMPs investigated here are limited. BP100 is an analog of the α-helical cecropin A-melittin hybrid AMP, Pep3.[6,38,39] Differing from Pep3 by only two amino acid residues (Trp1 and Val10 in Pep3 are replaced by Lys and Tyr, respectively, in BP100), a α-helical conformation for BP100 can be anticipated. Using circular dichroism, the adoption of this conformation by the peptide when in the presence of high POPG:POPC (2:1) concentrations was demonstrated.[40] For pepR, on the other hand, no data on the structural conformation adopted by this peptide are directly available. Derived from the α-helical RNA binding domain of the dengue virus capsid protein,[9] a α-helical conformation for pepR can however be postulated. The analysis of the BD trajectories generated for BP100 when confined within POPC (L_α), POPC:Chol (L_o), or POPG:POPC (L_α) pointed to the adoption of a α-helix by the peptide (see Figure 2). For pepR under the same conditions, the formation of a α-helix at the N-terminus of this peptide was revealed, whereas the C-terminus appeared to be less ordered (see Figure 3).

When determining the type of secondary structure adopted by a peptide, the backbone dihedral angles can be evaluated. Generally, the ϕ, ψ, and C_α dihedral angles are all considered. Based on the nature of the coarse-grained model used in this study, however, only the C_α dihedral angles of each AMP could be assessed. For an ideal α-helix, the C_α dihedral angle values are ~50°.[41] Based on the C_α dihedral angles recorded for each amino acid of BP100, which were observed to fluctuate between 50.8° and 58.2° (Figure 4A), it is clear that all the residues of this peptide are involved in the formation of a α-helical structure. For pepR, on the other hand, only the C_α dihedral angles for residues 2–27 were observed to fluctuate around 48.6° ± 5.2° (Figure 4B). This combined with RMSD values of ~2.6° shows that residues 2–27 retain a α-helical structure, which is terminated by Leu30. The remaining pepR C_α dihedral angles, at both ends of the peptide, deviated from 50° to varying degrees and exhibited RMSD values at least eight times larger than those in the helical region (Figure 4B). This is indicative of the remaining residues in the peptide not forming part of the α-helical segment. In fact, the 109.4° C_α dihedral angle at 32 (Figure 4B), which encompasses residues 32–35 of pepR, contributes toward the disordered appearance of the C-terminus of the peptide.

Although the detailed intramolecular atomic interactions occurring within each AMP under investigation could not be accurately represented using the implemented coarse-grained modeling approach, information on the overall peptide structure was still possible. The snapshots presented in Figures 5A and 5B are typical for BP100 and pepR, respectively, when simulated in any one of the three modeled membrane environments. For BP100, the charged and hydrophobic residues were observed to be distributed onto opposite regions of the structure (Figure 5A). This amphipathic arrangement, characteristic of Pep3[38,39] and a common feature of α-helical AMPs,[3,42] is known to play a key role in stabilizing the parallel adsorption and subsequent burial of such peptides into the membrane.[3,42] This is achieved through the interaction of the hydrophobic face of the AMPs with the lipid components of the membrane while the charged residues bind to the phospholipid head groups. Based on these observations, the amphipathic character of the simulated BP100 structure provides support for the parallel burying of this cationic peptide to phospholipid bilayers, particularly those modeling the anionic bacterial membrane.[8,40] Such an arrangement within the membrane environment, combined with the proposed interaction of one BP100 molecule (+6 at pH 7.4) with 5.6 negatively charged phospholipids at saturation,[8] can account for the reported neutralization of anionic bacterial membrane model surfaces and the *E. coli* cell surface when using the peptide at concentrations equivalent to and greater than MIC values.[7,8] Analysis of the simulated pepR structure (Figure 5B), on the other hand, demonstrated the distribution of charged and hydrophobic residues onto opposite regions of the structure only within certain portions within the peptide. These regions more than likely interact with the membrane in a manner equivalent to that discussed for BP100. However, considering the relatively large size of pepR and the predominance of charged (+12 at pH 7.4) and polar residues in its structure, it is unlikely that all the positive charges in the peptide will come into contact with the membrane surface. These unbound charges may consequently mask the overall surface net charge. This concept is supported by the fact that following the treatment of *E. coli* cells with pepR at concentrations equal to and above MIC values, an overcompensation in the bacterial wall surface charge was detected.[7]

To further assess the behavioral properties of BP100 and pepR, the dynamic properties of each AMP were also investigated. This was achieved by monitoring the local and global motions of each peptide when confined within the three modeled membrane environments.

As described in the "Structural Properties of BP100 and pepR" section, both BP100 and pepR tended to adopt specific conformations when confined within the membrane environment. To verify the described observations and to gain further insights into their overall structural properties, key structural elements were screened for each AMP throughout each of the simulated BD trajectories. By this screening method, insights into the local motions within each peptide were acquired.

For BP100 confined within the membrane environment, the formation of a α-helix was recorded. For an ideal α-helix, a 1.5 Å rise per residue exists.[43] Thus, a length of 16.5 Å may be expected for BP100. On this basis, the distance between the N- and C-terminal residues of the peptide when simulated in POPC (L_α), POPC:Chol (L_o), or POPG:POPC (L_α) was monitored (see Figure 6). Under the varying conditions, the average measured distance between the N- and C-terminal residues of BP100 (i.e., between Lys1 and Leu11) was found to be ~15.6 Å. This value is almost comparable with the 16.5 Å length expected for BP100 if in a α-helical conformation and is thus suggestive of BP100 adopting of a slightly compacted α-helix when in the different membrane environments.

When confined in the membrane environment, pepR was observed to adopt a distinctly different conformation from BP100, with its N-terminus always forming a α-helix and its C-terminus being less structured (see "Structural Properties of BP100 and pepR" section). So as to judge the maintenance of this conformation, the length of the N-terminal α-helix and the end-to-end distance between the N- and C-termini were screened for pepR throughout each of the simulated BD trajectories. The N-terminal α-helix of pepR was found to be 37.8 ± 4.9 Å, 37.6 ± 5.1 Å, and 37.9 ± 4.9 Å when simulated in POPC (L_α), POPC:Chol (L_o), and POPG:POPC (L_α), respectively. Taking into account the 1.5 Å rise per residue for an ideal α-helical structure,[43] 43.5 Å is the expected length for the pepR α-helix. Clearly, the N-terminal α-helix length values obtained from the BD simulation studies do not compare well with the expected theoretical value. Also, relative to the helix length values recorded for BP100 when simulated in the same modeled membrane systems, the deviations here were large. On close examination, it is clear that the calculated length of the pepR N-terminal α-helix when confined within each modeled membrane is comparable with the distance separating the membrane interfaces (see Table I). It is likely that in the process of the BD simulation, when each terminus of the long pepR α-helix comes in close proximity to each respective membrane interface, they are moved back to the membrane core by the enclosing potential. This, in conjunction with the inertial effects affecting the overall movement of the bulk of the pepR helix, may contribute to the observed bending in the peptide structure (see Figure 3). The deviations in the helix length recorded when simulating

pepR in the membrane may thus be explained by this behavior. It is important to note at this stage that during the optimization process, in which pepR was simulated in water, bending of the peptide structure was not detected (data not shown).

When measuring the distance separating the N- and C-termini of pepR when simulated in the membrane environment, similar distances to that described for the peptide's N-terminal α-helix (i.e., the distance between Lys2 and Leu30) were revealed. On average, the distance between Leu1 and Arg35 of pepR was 39.9 ± 8.1 Å, 39.6 ± 8.4 Å, and 40.1 ± 8.1 Å when simulated in POPC (L_α), POPC:Chol (L_o), and POPG:POPC (L_α), respectively. When in the vicinity of the membrane interface, residues 31–35 at the C-terminus of pepR are more than likely pushed back in the direction of the membrane core by the enclosing potential. This, coupled with the physical nature of the N-terminal α-helix described above, contributes toward the occasional formation of a turn at the C-terminus of the peptide (see Figures 3E, 3H, 3I, 3J, 3L, 3N, and 3O). As a result of this turn, Arg35 is brought closer to Leu1. The similarity in the values acquired when calculating the length of the pepR α-helix with those obtained when measuring the distance between Leu1 and Arg35 is thus a consequence of the formation of the turn at the C-terminus of the peptide. The larger deviations obtained when measuring the distance separating Leu1 and Arg35, however, are indicative of the C-terminus of pepR being less ordered relative to the rest of the peptide structure.

When considering the above-discussed results, it is clear that the fluctuations in the end-to-end distance and other significant intramolecular distances are greater in pepR relative to BP100. This is clearly evidenced by the difference in the magnitudes of the standard deviations obtained when calculating the various intramolecular distances for each peptide. These differences seem to be beyond what one can expect from the two different peptide lengths. Overall, this apparent behavioral difference may be attributed to the disordered C-terminal region in pepR described in the previous paragraph. When calculating the distance between Leu1 and Leu30 of pepR (not accounting for the disordered C-terminal region), values of 38.0 ± 5.1 Å, 37.8 ± 5.4 Å, and 38.9 ± 5.2 Å were obtained for the peptide when simulated in POPC (L_α), POPC:Chol (L_o), and POPG:POPC (L_α), respectively (graphical data not shown). The values obtained when calculating the distance between Leu1 and Arg35 of pepR when in POPC (L_α), POPC:Chol (L_o), and POPG:POPC (L_α) were 39.9 ± 8.1 Å, 39.6 ± 8.4 Å, and 40.1 ± 8.1 Å, respectively. Clearly, the standard deviations recorded when calculating the distance between Leu1 and Leu30 of pepR under the varying conditions are not as large as those obtained when calculating the distance between Leu1 and Arg35 of the peptide under the equivalent conditions. Such data once again illustrate the disordered nature of the C-terminus of pepR relative to the rest of the peptide structure. It is noteworthy that this C-terminal region, which is less than one-third of the whole pepR structure, produces such an effect.

The global motions of both BP100 and pepR when confined within the membrane environment were also explored to acquire further insights into the mode of action of each AMP. This was achieved by monitoring the localization and orientation of each peptide within the different modeled membrane systems.

From the density profiles presented in Figures 8 and 9, differences in the dispersion of the localization of BP100 and pepR when traversing POPC (L_α), POPC:Chol (L_o), or POPG:POPC (L_α) were detected. The overall motions of BP100 within the three different membrane environments revealed the existence of populations at ±10 Å from the bilayer center. This localization of the peptide approximately halfway across each membrane leaflet was in contrast to the localization of the pepR mass center around the core of each membrane model. Thus far, only the in-depth localization of BP100 in phospholipid bilayers has been reported.[8] In these biophysical studies, it was found that in the absence of saturation, BP100 tended to position itself 10.5 Å from the bilayer center. No significant alteration in its in-depth localization was detected on saturation, with the average position here being 11.2 Å from the bilayer center. The localization of BP100 within the membrane environment as established from the BD simulation studies is therefore in good agreement with the experimentally determined values.

When assessing the orientation of both BP100 and pepR in POPC (L_α), POPC:Chol (L_o), or POPG:POPC (L_α), equivalent trends were detected (see Figures 10 and 11). Overall, frequent fluctuations in the orientation of each AMP relative to the membrane normal were observed, with these fluctuations occurring over a wider domain of orientations for each peptide when in POPC (L_α) (Figures 10B and 11B) and POPC:Chol (L_o) (Figures 10D and 11D) relative to when in the thicker POPG:POPC (L_α) (Figures 10F and 11F). This was evidenced for both BP100 and pepR by tilt angles in the range of 90.0°–114.4°, as well as the large standard deviations generated when determining the tilt angle values. Generally, these observations more than likely reflect the existence of peptide populations in the lipid bilayer with no preferred orientation.

Taken as a whole, the differences in the localization and orientation of BP100 and pepR when traversing each of the simulated membrane models can be attributed to the greater mobility of the smaller BP100 chain across the membrane layer when compared with that of the larger pepR chain. Both AMPs were also observed to be more mobile when in the thinner membranes [i.e., POPC (L_α) and POPC:Chol (L_o)] relative to when in the thicker one [i.e., POPG:POPC (L_α)].

Biophysical studies have shown that the physicochemical composition of a lipid bilayer can play a role in determining the mode of action of AMPs. This can largely be attributed to the orientation adopted by the peptide relative to the membrane normal. Melittin and alamethicin, for example, have been shown to orientate parallel to the membrane normal at high water content. Cooling the samples below the main transition temperature prompted the axis of each peptide to move toward the membrane plane. For low water content, a parallel orientation of the helices relative to the membrane surface was suggested.[44,45] Yang et al.[46] also demonstrated that on increasing peptide/lipid ratios, the melittin helix orientation tended to move toward the membrane normal. This event was strongly influenced by the lipid composition of the bilayer and was most pronounced for the peptide in POPC in the L_α phase. Altogether, the perpendicular orientation relative to the membrane surface was conducive to the formation of a toroidal pore and a barrel-stave pore for melittin and alamethicin, respectively. When simulating BP100 and pepR in POPC (L_α), POPC:Chol (L_o), or POPG:POPC (L_α), no preference in the orientation of the helix of each peptide relative to the membrane surface was detected. Thus, the contribution of the membrane properties on the preferred orientation of each of these peptides in the lipid bilayer and the consequent insights into their probable mode of action was not possible. For pore formation to be considered, both BP100 and pepR would have to be sufficiently long to span the lipid membrane. When considering the length of BP100 (see "Local Peptide Motions" section), as well as the dimensions of each of the modeled membranes (see Table I), the formation of a pore by this peptide is unlikely. Rather, the adoption of a carpet mechanism[1,3] is more plausible for such a short peptide. For pepR, on the other hand, its length as recorded in the "Local Peptide Motions" section is comparable with the dimensions of each of the modeled membrane systems (see Table I). Thus, dependent on the transmembrane orientation of this peptide, it may simply destabilize the membrane or alternatively it may span the membrane resulting in the formation of either barrel-stave[47,48] or toroidal pores.[46] Recently, Castanho and coworkers found that following the treatment of *E. coli* cells with either BP100 or pepR at concentrations equivalent to or above their respective MIC values, membrane disruption and subsequently cell leakage occurred.[7] Based on the nature of the alterations on the surface of the bacterial cell envelope under these conditions, as viewed by AFM imaging, a carpet-like or detergent-like mechanism was proposed for both AMPs. Combining this experimental data with the above-discussed global Brownian motions of each AMP when simulated in the different membrane environments, the carpet-like or detergent-like mechanisms appear to be the likely adopted mode of action of BP100, and the same mechanisms cannot be ruled out for pepR.

A final consideration in the analysis of the BD trajectories generated for both BP100 and pepR was the extraction of the translational diffusion coefficients for each peptide when confined in POPC (L_α), POPC:Chol (L_o), or POPG:POPC (L_α) (Table II). Altogether, simulation of BP100 in the different membrane models presented a diffusion coefficient larger than that of pepR under the same conditions. In a recent study on the lateral diffusion of a variety of biomolecules in membranes, the diffusion coefficient was demonstrated to be inversely proportional to the radius of the diffusing body and to the thickness of the membrane.[49] Based on this, the larger diffusion coefficients obtained for BP100 in each of the three modeled membranes, when compared with those of pepR in the equivalent conditions, can be attributed to its smaller size. The decrease in the membrane width was found to further enhance the difference in the diffusion coefficients measured for each AMP. Moreover, the orientation of each AMP relative to the membrane normal may be an additional factor influencing the difference in magnitude in the diffusion coefficients obtained for each peptide when in the different membrane environments. When taking into account the drag experienced by each peptide when translationally diffusing across the different membrane environments, it should be borne in mind that a minimal drag would be experienced by each peptide if the tilt angle (θ_i) were 90°, whereas a maximal drag would be experienced by each peptide if the tilt angle (θ_i) was 0°. From the statistics of the tilt angles reported in the "Global Peptide Motions" section, both BP100 and pepR were observed to adopt tilt angles in the range of 90.0°–97.8° when in POPC (L_α) and POPC:Chol (L_o). For each AMP confined in POPG:POPC (L_α), on the other hand, the tilt angle values varied in the range of 103.0°–114.4°. On this basis it is clear that when confined in POPC (L_α) and POPC:Chol (L_o), each AMP experiences less drag relative to when confined in POPG:POPC (L_α). Thus, the propensity of each peptide to orientate at an angle around 90° relative to the membrane normal when in POPC (L_α) and POPC:Chol (L_o) may explain why the diffusion coefficients of both BP100 and

pepR are higher in these two membrane environments relative to when in POPG:POPC (L_α) (see Table II).

Although experimental data on the lateral diffusion of either BP100 or pepR in the membrane environment are unavailable, comparisons with the diffusion coefficients obtained for other similarly sized peptides can be made. For the 21-residue CPP, Pep-1, diffusion coefficients ranging from 0.3×10^{-8} to 1.1×10^{-8} cm^2/s were reported for peptide clusters of varying sizes migrating along the surface of POPC giant unilamellar vesicles.[50] Taking into account the inverse relationship between the diffusion coefficient and the radius of the diffusing body,[49] a single Pep-1 molecule will display a larger diffusion coefficient than that of the Pep-1 clusters. Bearing this in mind, the magnitudes of the diffusion coefficients measured for both BP100 and pepR when simulated in POPC (L_α) (see Table II) may be considered reasonable when compared with that of the diffusing Pep-1 clusters. Furthermore, when considering the discussed differences in the diffusion of each AMP in the different membrane environments, the remaining diffusion coefficient values listed in Table II are anticipated to be acceptable.

CONCLUSIONS

In this work, the mode of action of BP100 and pepR was explored by the BD simulation of a coarse-grained model of peptide in an environment reproducing the phospholipid bilayer. The simplicity of the mean-field potentials used to reproduce physically different model PC membrane systems, combined with the use of the coarse-grained peptide model, allowed for feasible, long-time range, and easy to implement simulations.

With the appropriate choice of parameters, data on the structural and dynamic properties of both BP100 and pepR when confined in the different model membranes were successfully recovered from each of the simulated BD trajectories. BP100 was found to adopt a α-helical conformation when confined within the membrane environment. For pepR, on the other hand, the formation of an N-terminal α-helix and an unstructured C-terminus was detected. Differences in the global motions of each AMP when in the membrane were also revealed. BP100 was observed to localize with no preferred orientation approximately halfway across each membrane leaflet, whereas pepR tended to localize near the lipid bilayer core with no preferred orientation. The BD simulation studies also allowed for the determination of the lateral diffusion coefficients of each AMP. As a result of the size difference between the two peptides, BP100 was observed to diffuse more rapidly than pepR across each of the modeled membranes. The membrane width was found to play an additional role in determining the lateral diffusion coefficient of each peptide when in the membrane.

In conclusion, the method used in this study allowed for the description of the conformational and dynamic properties of both BP100 and pepR when confined within different membrane environments. Not only did the BD simulation studies allow for the corroboration of what little experimental data was available but also provided some insights into the possible mechanisms of action adopted by each AMP. However, details on the initial peptide-membrane association events could not be tackled using the implemented membrane model. This limitation in the computational system used to model the behavioral properties of each AMP prompts the future development of a mean-field potential to describe the interface region of the membrane environment. One prospective example would involve the incorporation of a model that describes the electrostatic interactions at the membrane interface region. Such work constitutes our ongoing desire to develop a simple and easy-to-implement simulation method to investigate the mode of action of membrane-active peptides such BP100 and pepR.

REFERENCES

1. Brogden, K. A. Nat Rev Microbiol 2005, 3, 238–250.
2. Zasloff, M. Nature 2002, 415, 389–395.
3. Yeaman, M. R.; Yount, N. Y. Pharmacol Rev 2003, 55, 27–55.
4. Melo, M. N.; Ferre, R.; Castanho, M. A. Nat Rev Microbiol 2009, 7, 245–250.
5. Andreu, D.; Ubach, J.; Boman, A.; Wahlin, B.; Wade, D.; Merrifield, R. B.; Boman, H. G. FEBS Lett 1992, 296, 190–194.
6. Badosa, E.; Ferre, R.; Planas, M.; Feliu, L.; Besalu, E.; Cabrefiga, J.; Bardaji, E.; Montesinos, E. Peptides 2007, 28, 2276–2285.
7. Alves, C. S.; Melo, M. N.; Franquelim, H. G.; Ferre, R.; Planas, M.; Feliu, L.; Bardaji, E.; Kowalczyk, W.; Andreu, D.; Santos, N. C.; Fernandes, M. X.; Castanho, M. A. J Biol Chem 2010, 285, 27536–27544.
8. Ferre, R.; Melo, M. N.; Correia, A. D.; Feliu, L.; Bardaji, E.; Planas, M.; Castanho, M. Biophys J 2009, 96, 1815–1827.
9. Ma, L.; Jones, C. T.; Groesch, T. D.; Kuhn, R. J.; Post, C. B. Proc Natl Acad Sci USA 2004, 101, 3414–3419.
10. Appelt, C.; Eisenmenger, F.; Kuhne, R.; Schmieder, P.; Soderhall, J. A. Biophys J 2005, 89, 2296–2306.
11. Belohorcova, K.; Davis, J. H.; Woolf, T. B.; Roux, B. Biophys J 1997, 73, 3039–3055.
12. Huang, W. N.; Sue, S. C.; Wang, D. S.; Wu, P. L.; Wu, W. G. Biochemistry 2003, 42, 7457–7466.
13. Khandelia, H.; Kaznessis, Y. N. Peptides 2006, 27, 1192–1200.
14. Khandelia, H.; Kaznessis, Y. N. Biochim Biophys Acta 2007, 1768, 509–520.
15. Mihailescu, D.; Smith, J. C. Biophys J 2000, 79, 1718–1730.

16. Murzyn, K.; Pasenkiewicz-Gierula, M. J Mol Model 2003, 9, 217–224.
17. Saiz, L.; Bandyopadhyay, S.; Klein, M. L. Biosci Rep 2002, 22, 151–173.
18. Shepherd, C. M.; Vogel, H. J.; Tieleman, D. P. Biochem J 2003, 370, 233–243.
19. Huertas, M. L.; Cruz, V.; Cascales, J. J.; Acuna, A. U.; Garcia de la Torre, J. Biophys J 1996, 71, 1428–1439.
20. Tozzini, V. Curr Opin Struct Biol 2005, 15, 144–150.
21. Chang, C.-E.; Shen, T.; Trylska, J.; Tozzini, V.; McCammon, J. A. Biophys J 2006, 90, 3880–3885.
22. Cheng, Y.; Chang, C. E.; Yu, Z.; Zhang, Y.; Sun, M.; Leyh, T. S.; Holst, M. J.; McCammon, J. A. Biophys J 2008, 95, 4659–4667.
23. Fernandes, M. X.; Huertas, M. L.; Castanho, M. A.; Garcia de la Torre, J. Biochim Biophys Acta 2000, 1463, 131–141.
24. Fernandes, M. X.; Garcia de la Torre, J.; Castanho, M. A. R. B. J Phys Chem B 2000, 104, 11579–11584.
25. Muller-Plathe, F. ChemPhysChem 2002, 3, 755–769.
26. Tozzini, V.; McCammon, J. A. Chem Phys Lett 2005, 413, 123–128.
27. Trylska, J.; Tozzini, V.; McCammon, J. A. Biophys J 2005, 89, 1455–1463.
28. Iniesta, A.; de la Torre, J. G. J Chem Phys 1990, 92, 2015–2018.
29. Ermak, D. L.; McCammon, J. A. J Chem Phys 1978, 69, 1352–1360.
30. Rotne, J.; Prager, S. J Chem Phys 1969, 50, 4831–4837.
31. Yamakawa, H. J Chem Phys 1970, 53, 436–443.
32. Wade, R. C.; Davis, M. E.; Luty, B. A.; Madura, J. D.; McCammon, J. A. Biophys J 1993, 64, 9–15.
33. Zaccai, G.; Buldt, G.; Seelig, A.; Seelig, J. J Mol Biol 1979, 134, 693–706.
34. Cady, S. D.; Goodman, C.; Tatko, C. D.; DeGrado, W. F.; Hong, M. J Am Chem Soc 2007, 129, 5719–5729.
35. Henriques, S. T.; Quintas, A.; Bagatolli, L. A.; Homble, F.; Castanho, M. A. Mol Membr Biol 2007, 24, 282–293.
36. Elmore, D. E. FEBS Lett 2006, 580, 144–148.
37. Zhao, W.; Rog, T.; Gurtovenko, A. A.; Vattulainen, I.; Karttunen, M. Biophys J 2007, 92, 1114–1124.
38. Cavallarin, L.; Andreu, D.; San Segundo, B. Mol Plant Microbe Interact 1998, 11, 218–227.
39. Ferre, R.; Badosa, E.; Feliu, L.; Planas, M.; Montesinos, E.; Bardaji, E. Appl Environ Microbiol 2006, 72, 3302–3308.
40. Melo, M. N. A study on the mode of action of clinically relevant antimicrobial peptides. In Department of Chemistry and Biochemistry, University of Lisbon: Lisbon, 2010; pp 1–214.
41. Ramakrishna, C.; Soman, K. V. Int J Pept Protein Res 1982, 20, 218–237.
42. Jenssen, H.; Hamill, P.; Hancock, R. E. Clin Microbiol Rev 2006, 19, 491–511.
43. Ambroggio, E. E.; Separovic, F.; Bowie, J. H.; Fidelio, G. D.; Bagatolli, L. A. Biophys J 2005, 89, 1874–1881.
44. Vogel, H. Biochemistry 1987, 26, 4562–4572.
45. Vogel, H.; Jahnig, F.; Hoffmann, V.; Stumpel, J. Biochim Biophys Acta 1983, 733, 201–209.
46. Yang, L.; Harroun, T. A.; Weiss, T. M.; Ding, L.; Huang, H. W. Biophys J 2001, 81, 1475–1485.
47. Shai, Y. Biochim Biophys Acta 1999, 1462, 55–70.
48. Shai, Y.; Oren, Z. Peptides 2001, 22, 1629–1641.
49. Gambin, Y.; Lopez-Esparza, R.; Reffay, M.; Sierecki, E.; Gov, N. S.; Genest, M.; Hodges, R. S.; Urbach, W. Proc Natl Acad Sci USA 2006, 103, 2098–2102.
50. Sharonov, A.; Hochstrasser, R. M. Biochemistry 2007, 46, 7963–7972.